Dynamic Analysis for VSG-Based Power Flow Control Applied to DG Systems

Thiago F. do Nascimento
Federal University of Rio Grande do Norte (UFRN)
Natal, Brazil
Email: figueiredo.21@hotmail.com

Andres O. Salazar
Federal University of Rio Grande do Norte (UFRN)
Natal, Brazil
Email: andres@dca.ufrn.br

***Resumo*—The integration of distributed generation (DG) systems based on renewable energy sources (RES) by using power converters is an emerging technology in modern power systems. Among the control strategies applied to this new configuration, the virtual synchronous generator (VSG) approach has proven to be an attractive solution due providing suitable dynamic performance. Thus, this paper presents a dynamic analysis of grid-tied converters controlled by using VSG concept. This analysis is based on a dynamic model that describes the DG power flow transient characteristics. Based on this model, the grid impedance parameters variation effects on the VSG controllers dynamic performance are discussed. Simulation results are presented to evaluate the effectiveness of the theoretical analysis performed.**

***Keywords* – Distributed generation, dynamic analysis, renewable energy sources, virtual synchronous generator.**

I. Introduction

Because environmental concerns, the development of DG systems based in RES, such as wind turbines and/or photovoltaic systems, have increase in a rapid pace in the recent years. Moreover, the DG systems provide other advantages, such as greater robustness and reliability. In general, these DG units are interconnect to the power grid by using grid-tied power converters that employ dedicated control strategies for regulating the system power flow. These control strategies applied to grid-tied converters allow them to operate as controlled current sources or controlled voltage sources for providing grid support [1]. However, the grid-tied converters operating as controlled voltage sources can provide suitable performance to the power system with DG systems high penetration level, and also allows the DG units to operate in grid-connected or islanded modes [2]. Among the control strategies used to applied this operation mode to the grid-tied converters, the VSG strategy has gained more interest due to its operation similarity with conventional synchronous generators (SG) that actively participate in the system power flow regulation to provide a suitable power balance[4].

Since VSG is implemented in software, its parameters can be designed using the desired dynamic performance and stability criteria. Thus, some dynamic analysis methods to improve the VSG strategy performance have been proposed in the literature [6]-[9]. In [6] and [7], the proposal was the usage of the Root-Locus Method (RLM) to perform the dynamic analysis of the closed-loop system. Based on this analysis, the control parameters were adjusted to meet the desired dynamic performance. However, the DG power flow transient characteristics are not considered in system dynamic modeling, thus the projected VSG parameters require further adjustments to obtain the desired dynamic response. The Pole Allocation Design Method (PADM) is employed in [8] to perform dynamic analysis of the active power flow. However, the transient effect related to the system parameters variation is not also considered. Besides, the reactive power controller has not been implemented in this work. In [9], the closed-loop transfer function of active and reactive power control was derived for dynamic analysis by using Frequency Response Design Method (FRDM). However, dynamic analysis was used only to ensure power tracking without considering the required performance to system transient response.

The DG power flow modeling neglecting its transient characteristics related to system parameters may not be appropriate to evaluate the control performance under grid impedance variation effect [10]. Thus, this paper proposes a dynamic analysis based on a mathematical modeling considering the transient characteristics which depends on the grid impedance parameters. This analysis is performed using the RLM and described the relationship between the power flow dynamic response and grid impedance variation, which can be applied to realize desired dynamic performance through VSG control parameters design. Finally, simulation results verify the theoretical analysis effectiveness.

This paper is organized as follows. Section II presents the VSG control operation principle. The DG power flow small-signal model is presented in Section III. The analysis of the transient and steady state responses related to DG power flow are presented in detail in Section IV. The analysis of the closer-loop power control is presented in Section V. The simulation results and performance analysis are presented in Section VI, while Section VII concludes this paper.

II. VSG Strategy Operation Principle

Fig. 1 presents the topology and block diagram of the VSG strategy applied to the DG interconnection system. A three-phase voltage-source converter (VSC) connected to point of common coupling (PCC) through a LC-filter composed by inductor L_i and capacitor C_f, wherein r_i is the intrinsic resistance of the filter inductor, implements the VSG algorithm.

https://doi.org/10.53316/sepoc2021.037

A DC voltage source implements the primary source of the grid-tied converter (i.e., photovoltaic or wind power system). In this diagram, the power grid is composed by sinusoidal voltage sources connected to PCC through a grid impedance that consists in inductor L_g and resistor R_g. The linear load is composed by series connected inductor L_l and resistor R_l and is controlled by switche K_1 to implement different operational scenarios.

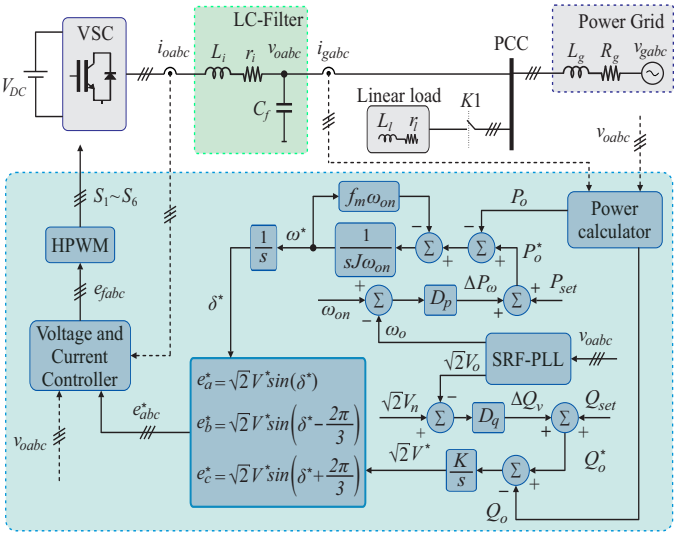

Figura 1. Topology of the DG interconnection system with VSG control strategy.

According to Fig.1, the VSG strategy implemented in this work is composed by a DG power flow control loop in cascaded with a PCC voltage and VSC output current control loop. The outer loop regulates the DG power flow provided to the power grid. The active power controller consists in the emulation of the synchronous generator swing equation given by:

$$P_o^*(t) - P_o(t) - f_m\omega_{on}\frac{d\delta(t)}{dt} = J\omega_{on}\frac{d^2\delta(t)}{dt^2}, \quad (1)$$

where J is the inertia moment, f_m the friction factor, ω_{on} the system nominal angular frequency and δ corresponds to the system load angle. The VSG reactive power controller is based on the emulation of the following dynamic equation:

$$Q_o^*(t) - Q_o(t) = \frac{1}{K}\frac{dV_o(t)}{dt}, \quad (2)$$

where K represents a control integral gain. The DG power flow loop also employs droop control, which adjust the active and reactive power reference value according to grid frequency and PCC voltage, respectively. Thus, the active and reactive power reference consists in $P_o^* = P_{set} + \Delta P_\omega$ and $Q_o^* = Q_{set} + \Delta Q_v$, respectively, in which $\Delta P_\omega = D_p(\omega_n - \omega_o)$ and $\Delta Q_v = D_q(V_n - V_o)$. The D_p and D_q terms are the droop gains. The ω_n and V_n terms represent the system nominal frequency and voltage, respectively, and ω_o and V_o are estimation provided by a synchronous reference frame phase-locked loop (SRF-PLL).

The PCC voltage reference e_{abc}^* is provided by DG power flow controllers (see Fig. 1). The phase-angle reference value δ^* is determined by the active power controller, while the amplitude reference value $\sqrt{2}V^*$ is provided by the reactive power controller. The reference voltages e_{fabc} determined by the inner loop is applied to the HPWM strategy [11], which determine the drive signals of power converter $S1 - S6$. The inner loop controllers can be significantly faster than the DG power flow controllers of the outer loop, and hence its dynamics is neglected in the proposed analysis in this work.

III. DG Power Flow Modeling

The grid-tied converter controlled by the VSG strategy operates as a controllable voltage source connected to the PCC. Thus, the balanced three-phase system of Fig. 1 can be represented by equivalent circuit illustrated in Fig. 2.

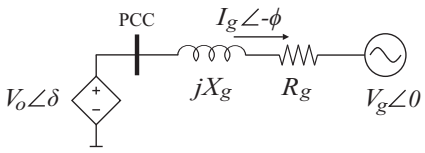

Figura 2. Equivalent circuit of the grid-tied converter.

According to Fig. 2, the phasor currents provided to the power grid can be obtained as follows:

$$\dot{I}_g = \frac{\dot{V}_o - \dot{V}_g}{R_g + jX_g}, \quad (3)$$

where $\dot{V}_g = V_g\angle 0^\circ$ and $\dot{V}_o = V_o\angle\delta$ represent the phasors of the power grid and PCC voltages, respectively. Thus, the DG output complex power (S_o) can be calculated as:

$$\begin{aligned} S_o = 3\dot{V}_o\overline{\dot{I}}_g &= 3\dot{V}_o\left(\frac{\overline{\dot{V}}_o - \overline{\dot{V}}_g}{R_g - jX_g}\right) \\ &= 3\left(\frac{V_o^2 - V_oV_g(cos(\delta) + jsin(\delta))}{R_g - jX_g}\right), \end{aligned} \quad (4)$$

where $\overline{\dot{V}}_o$, $\overline{\dot{V}}_g$, and $\overline{\dot{I}}_g$ represent the conjugate phasors of $\dot{V}_o$, $\dot{V}_g$, and $\dot{I}_g$, respectively. However, for a predominantly inductive grid impedance, that is $R_g \approx 0$, (4) can be rewritten as:

$$S_o \approx \frac{3V_oV_gsin(\delta)}{X_g} + j3\left(\frac{V_o^2 - V_gV_ocos(\delta)}{X_g}\right), \quad (5)$$

in which

$$P_o = \frac{3V_oV_gsin(\delta)}{X_g}, \quad (6)$$

$$Q_o = 3\left(\frac{V_o^2 - V_gV_ocos(\delta)}{X_g}\right), \quad (7)$$

represent the active and reactive power instantaneous values provided to the power grid, respectively. For small disturbances around the operating point, (6) and (7) can be linearized as reported in [9], resulting in the following expressions:

$$\hat{P}_o(s) = \frac{3V_{on}V_{gn}}{X_g}\hat{\delta}(s), \quad (8)$$

$$\hat{Q}_o(s) = \frac{3V_{on}}{X_g}\hat{V}_o(s), \tag{9}$$

where V_{gn} and V_{on} represent the grid and PCC voltage nominal values, respectively. The models described in (8) and (9) represent direct relationship between active power ($\hat{P}_o$) and load angle ($\hat{\delta}$) variations, as well as between the VSG reactive power variation ($\hat{Q}_o$) with PCC voltage variation ($\hat{V}_o$). However, they represent only the power flow dynamic in steady-state, which reduces its applications in systems with amount large of grid-tied power converters [10]. Thus, to analyze system transient behavior a more rigorous mathematical model are needed. Based on this idea, the modeling applied for the DG power flow that describes the dynamics corresponding to the relations P_o/δ and Q_o/V_o, is be based on the methodology developed in [10]. Therefore, for a grid impedance with inductive profile (see Fig. 1), the small-signal ac model of the active power provided to the power grid can be given by:

$$G_P(s) = \frac{\hat{P}_o(s)}{\hat{\delta}(s)} = \frac{h_p}{s^2 + \frac{2R_g}{L_g}s + \frac{R_g^2+(\omega_g L_g)^2}{L_g^2}}, \tag{10}$$

in which

$$h_p = \frac{3V_{on}V_{gn}}{L_g^2}(R_g sin(\delta_n) + \omega_g L_g cos(\delta_n)). \tag{11}$$

The ω_g and δ_n terms in (10) represent the nominal values of the grid angular frequency and load angle, respectively. By using similar procedure, the small-signal ac model of the reactive power delivered to the power grid can be given by:

$$G_Q(s) = \frac{\hat{Q}_o(s)}{\hat{V}_o(s)} = \frac{h_q}{s^2 + \frac{2R_g}{L_g}s + \frac{R_g^2+(\omega_g L_g)^2}{L_g^2}}, \tag{12}$$

in which

$$h_q = \frac{3}{L_g^2}(\omega_g L_g(2V_{on} - V_{gn}cos(\delta_n)) - R_g V_{gn} sin(\delta_n)). \tag{13}$$

The transfer functions in (10) and (12) represent more complete models that describe the system power flow dynamic behavior in relation to the system parameters.

IV. DG Power Flow Dynamic Analysis

The transfer functions described in (10) and (12) represent second-order systems. On the other hand, the transfer function that describes the dynamic behavior of typical second-order systems is given by [12]:

$$G(s) = \frac{\omega_n^2}{s^2 + 2\xi\omega_n s + \omega_n^2}, \tag{14}$$

where ξ and ω_n represent the damping ratio and the natural frequency, respectively. Thus, by matching the dynamic models $G_P(s)$ and $G_Q(s)$ to the transfer function described in (14), natural frequency (ω_n) and the damping ratio (ξ) related to these models can be calculated as follows:

$$\omega_n = \frac{\sqrt{R_g^2 + (\omega_g L_g)^2}}{L_g}, \tag{15}$$

$$\xi = \frac{R_g}{\sqrt{R_g^2 + (\omega_g L_g)^2}}. \tag{16}$$

Therefore, the DG power flow dynamic behavior is influenced by the grid impedance and angular frequency parameters. The poles of the transfer function in (14) are computed as follows:

$$s_{1,2} = -\xi\omega_n \pm \omega_n\sqrt{\xi^2 - 1} = -\frac{R_g}{L_g} \pm j\omega_g. \tag{17}$$

The poles given in (17) are complex with real part always negative, which indicates a DG power flow with under-damped response and stable. Besides, real part location varies as a function of the grid impedance parameters, while the imaginary part is equal to the grid angular frequency.

A. Transient Response Analysis

The systems parameters influence on the DG power flow transient response can be evaluated by specifications associated with under-damped responses, which are defined as rise time ($T_{r0-100\%}$), peak time (T_p), percent overshoot ($\%OS$), and settling time ($T_{s2\%}$). Their values are computed as follows [12]:

$$\begin{aligned} T_{r0-100\%} &= \frac{\pi - cos^{-1}(\xi)}{\omega_n\sqrt{1-\xi^2}} \\ &= \frac{1}{\omega_g}\left[\pi - cos^{-1}\left(\frac{R_g}{\sqrt{R_g^2 + (\omega_g L_g)^2}}\right)\right], \end{aligned} \tag{18}$$

$$T_p = \frac{\pi}{\omega_n\sqrt{1-\xi^2}} = \frac{\pi}{\omega_g}, \tag{19}$$

$$\begin{aligned} \%OS &= e^{-\left(\xi\pi/\sqrt{1-\xi^2}\right)} \times 100 \\ &= e^{-(R_g\pi/\omega_g L_g)} \times 100, \end{aligned} \tag{20}$$

$$T_{s2\%} = \frac{4}{\xi\omega_n} = \frac{4L_g}{R_g}. \tag{21}$$

According to equations above, the peak time value depends only on the grid angular frequency, while the values of the other specifications also depend on the grid impedance. Fig. 3(a) and (b) shows the percent overshoot, settling time and rise time, respectively, for different X/R ratio values. According to Fig. 3(a), when X/R ratio increases from 1.25 to 5.1, the percent overshoot and settling time increases from 8.2% to 53.5%, while the settling time increases from 0.013 to 0.053 s, approximately, which represents a degradation on the DG power flow transient performance. On the other hand, according to Fig. 3(b), for the same X/R ratio variation, the rise time decreases from 6.0 to 4.7 ms, approximately, which may represent an improvement on the DG power flow transient performance.

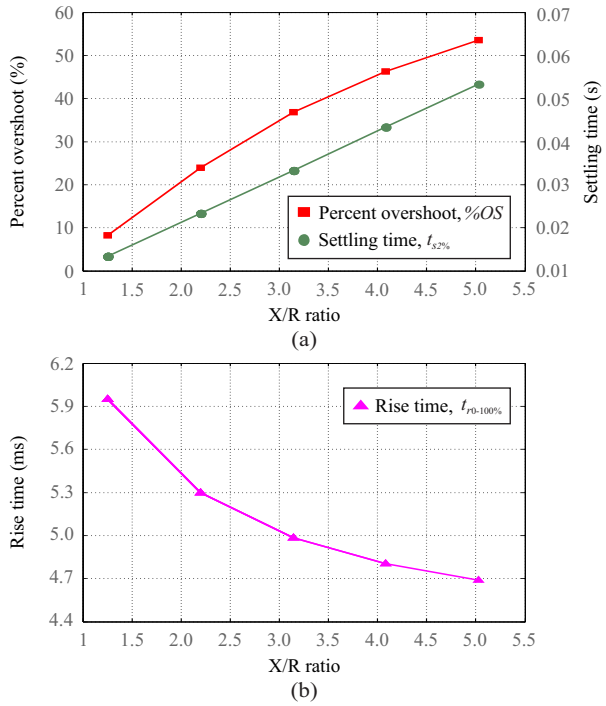

Figura 3. Transient specifications when the X/R ratio varies (a) Percent overshoot and settling time (b) Rise time.

B. Steady-State Response Analysis

The DG power flow steady-state response can be evaluated by using the error specifications for unity feedback systems. Since the closed-loop system is stable, these specifications can be obtained by final value theorem [12]. Thus, for a step imput, steady-state error values are defined as:

$$e_p(\infty) = \frac{1}{1 + \lim_{s\to 0} G_P(s)}, \tag{22}$$

$$e_q(\infty) = \frac{1}{1 + \lim_{s\to 0} G_Q(s)}, \tag{23}$$

where the $\lim_{s\to 0} G_P(s)$ and $\lim_{s\to 0} G_Q(s)$ terms represent static gains and are computed as:

$$\lim_{s\to 0} G_P(s) = \frac{3V_{on}V_{gn}}{R_g^2 + X_g^2}[R_g sin(\delta_n) + X_g cos(\delta_n)], \tag{24}$$

$$\lim_{s\to 0} G_Q(s) = \frac{3}{R_g^2 + X_g^2}[X_g(2V_{on} - V_{gn}cos(\delta_n)) - R_g V_{gn} sin(\delta_n)], \tag{25}$$

where $X_g = \omega_g L_g$. Applying the approximations $sin(\delta_n) \approx \delta_n$ and $cos(\delta_n) \approx 1$, and then assuming $R_g = 0$ and $V_{on} \approx V_{gn}$, the linearized models described in (8) and (9) are equal to the static gains given in (24) and (25), respectively, which indicates that these models are a special condition of (10) and (12), respectively.

Fig. 4 shows the steady-state error values for different X/R ratio values. According to Fig. 4, the error values for active and reactive power loop increases, when X/R ratio increases, which represents a degradation on the DG power flow steady-state response. However, the active and reactive power errors present small variations.

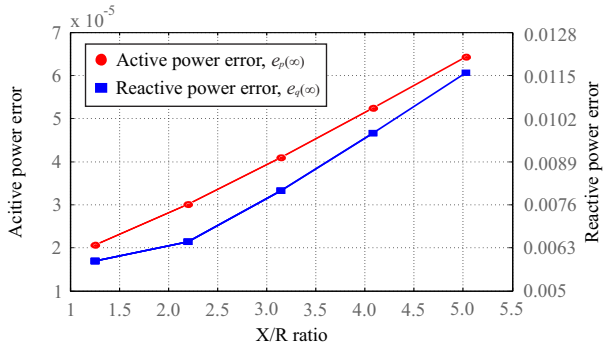

Figura 4. Active and reactive error values when the X/R ratio varies.

V. VSG-Based Power Flow Control

Fig. 5 shows the active and reactive power control loops, where the dynamic of the voltage and current control loops were neglected.

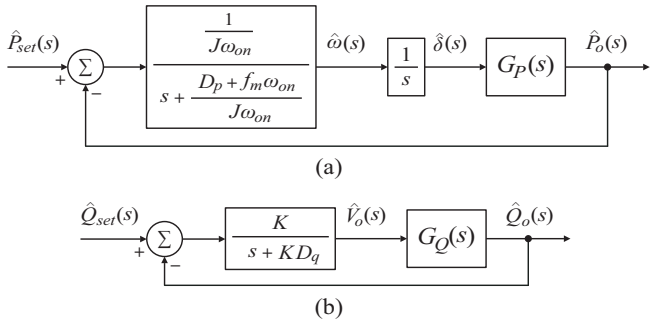

Figura 5. Control Loop. (a) Active power (b) Reactive power.

A. Active Power Control

According to block diagram of the Fig. 5(a), the closed-loop transfer function of active power control loop can be given by:

$$T_P(s) = \frac{\hat{P}_o(s)}{\hat{P}_{set}(s)} = \frac{a_0}{s^4 + a_3 s^3 + a_2 s^2 + a_1 s + a_0}, \tag{26}$$

in which

$$a_3 = \frac{L_g\left(D_p + f_m\omega_n\right) + 2J\omega_n R_g}{J\omega_n L_g}, \tag{27}$$

$$a_2 = \frac{2L_g R_g\left(D_p + f_m\omega_n\right) + J\omega_n\left(R_g^2 + (\omega_g L_g)^2\right)}{J\omega_n L_g^2}, \tag{28}$$

$$a_1 = \frac{\left(D_p + f_m\omega_n\right)\left(R_g^2 + (\omega_g L_g)^2\right)}{J\omega_n L_g^2}, \tag{29}$$

$$a_0 = \frac{h_p}{J\omega_n}. \tag{30}$$

The polynomial characteristic of the transfer function described in (26) has four poles which localization depends of the system grid impedance parameters. Considering the active power controller gains and system parameters listed in Table I, the X/R ratio variation effect in the location of the closed-loop poles are presented in Fig. 6(a). The closed-loop active power control has two complex dominant poles, which corresponds to the required performance, and two complex non-dominant poles furthest to the origin. When X/R ratio increases, the non-dominant poles are closer to the imaginary axis, which increases its effect in the system dynamic behavior, resulting in a more oscillatory transient response. On the other hand, the dominant poles are closer to the real axis, which can result in a more dampened transient response. Therefore, the grid impedance parameters variation can affect the active power controller dynamic performance.

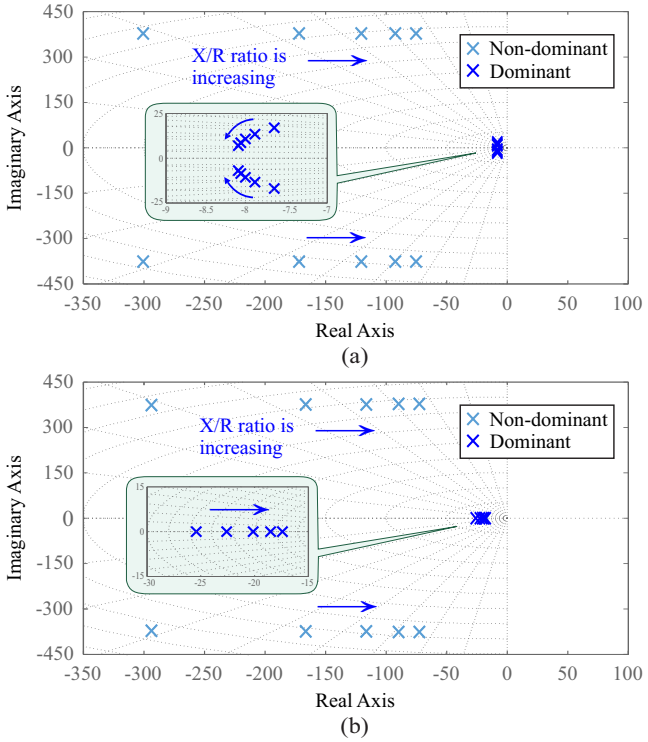

Figura 6. Closed-loop poles when X/R ratio varies (a) VSG active power control loop (b) VSG reactive power control loop.

B. Reactive Power Control

From the block diagram of Fig. 5(b), the closed-loop transfer function of reactive power control loop can be written as:

$$T_Q(s) = \frac{\hat{Q}_o(s)}{\hat{Q}_{set}(s)} = \frac{b_0}{s^3 + b_2 s^2 + b_1 s + b_0}, \tag{31}$$

in which

$$b_2 = \frac{KD_q L_g + 2R_g}{L_g}, \tag{32}$$

$$b_1 = \frac{2KD_q L_g R_g + R_g^2 + (\omega_g L_g)^2}{L_g^2}, \tag{33}$$

$$b_0 = \frac{KD_q\left(R_g^2 + (\omega_g L_g)^2\right) + Kh_q L_g^2}{L_g^2}. \tag{34}$$

The polynomial characteristic of the transfer function given in (31) has three poles with localization depends of the system grid impedance parameters. Fig. 6(b) shows the effect of the X/R ratio variation in the closed-loop poles for VSG reactive power control. The closed-loop reactive power control has one real dominant poles, which represents the desired performance, and two complex non-dominant poles furthest to the origin. With increasing X/R ratio the non-dominant poles are closer to the imaginary axis, while the dominant pole are closer to the origin, which results in a more slow transient response. Therefore, the grid impedance parameters variation can also affect the reactive power controller dynamic performance.

VI. Simulation Results

In this paper, the VSG grid-tied system topology presented in Fig. 1 is implemented in PSIM. The simulation study employs the parameters described in Table I.

Tabela I
DG System Parameters

Parameters	Value	Parameters	Value
DC-Link voltage V_{DC}	900 V	Load resistance R_l	30 Ω
Grid voltage V_g	127 V rms	Grid inductor L_g	5 mH
Grid frequency ω_{gn}	$2\pi 60$ rad/s	Grid resistance R_g	0.6 Ω
Rated power	10 kVA	Droop coefficient D_p	1326
Switching frequency f_s	10 kHz	Inertia moment J	0.364
Filter inductor L_i	3.5 mH	Friction factor f_m	2.41
Intrinsic resistance r_i	0.1 Ω	Droop coefficient D_q	556.8
Filter capacitor C_f	10 μF	Integral gain K	0.054
Load inductor L_l	80 mH		

A. Performance Analysis for Grid Impedance Variation

Figs. 7(a) and (b) present the VSG active and reactive power controllers dynamic performance under the system grid impedance variation effect considering an active power step variation between 0 and 10 kW with the reactive power set in 0 and reactive power step variation between 0 and 10 kvar with the active power set in 0, respectively. According to Fig. 7(a) and (b), the active and reactive power converge to their reference value accurately, which represents low influence on the active and reactive power controllers steady-state performance. However, 50% variations in X/R ratio significantly modified the these controllers transient performance. For $0.5X/R$ transient responses were more oscillatory, while $1.5X/R$ resulted in more dampened transient responses with longer rising times. Therefore, as discussed in Sections IV and V, a grid impedance variation can influence in the DG power flow control dynamic performance.

B. Performance Analysis for Load Variation on the PCC

Figs. 8(a) and (b) depict the VSG active and reactive power controllers dynamic performance under the load variation effect on the system PCC, when the active power is set in

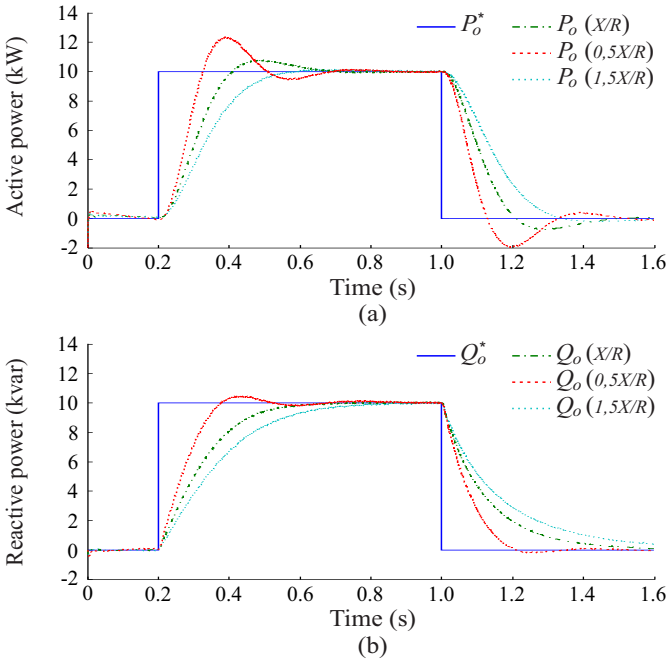

Figura 7. Power regulation with variation of X/R ratio (a) Active power (b) Reactive power

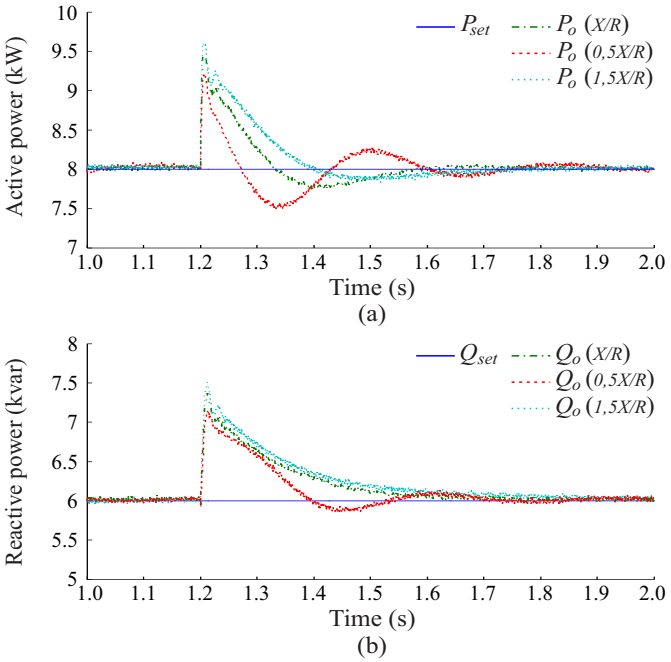

Figura 8. Power regulation with load variation for different X/R ratio values (a) Active power (b) Reactive power

8 kW and the reactive power is set in 6 kvar, simultaneously. At $t = 1.2$ s, the linear load is interconnected to the PCC during the system operation in steady-state for different grid impedance X/R ratio values. Again, for $0.5X/R$ transient responses were more oscillatory and for $1.5X/R$ transient responses were more dampened. In both cases, the active and reactive power converge again to their reference values accurately. Therefore, a grid impedance variation also influences in the DG power flow controllers dynamic performance under a load variation in the PCC.

VII. Conclusion

This paper presented a dynamic analysis based on the transient and steady-state response specifications to evaluate the dynamic behavior of the power flow in DG systems. Besides, the closed-loop poles behavior was analyzed for the VSG power flow control by using the Poles-Zeros Map. This analysis can be employed for VSG control parameters design in order to improve the system power flow dynamic performance. Simulations were performed in order to validate the proposed dynamic analysis. Power and load variations with different grid impedance values were simulated and the analysis was capable to demonstrate the its influence on the power controllers performance. Therefore, the results presented prove the effectiveness of this dynamic analysis in DG systems controlled by VSG.

Acknowledgment

The authors would like to thank the CAPES (Coordenação de Aperfeiçoamenteo de Pessoal de Nível Superior) and CNPq (Conselho Nacional de Pesquisa).

Referências

[1] J. Rocabert and A. Luna and F. Blaabjerg and P. Rodríguez, "Control of power converters in AC microgrids," in IEEE Transactions on Power Electronics, vol. 27, no. 11, pp. 4734-4749, Nov. 2012.

[2] Z. Shuai, Y. Sun, Z. J. Shen, W. Tian, C. Tu, Y. Li, X. Yin, "Microgrid stability: classification and a review," in Renewable and Sustainable Energy Reviews, vol. 58, pp. 167-179, May 2016.

[3] A. M. Azmy and I. Erlich, "Impact of distributed generation on the stability of electrical power system," in IEEE Power Engineering Society General Meeting, 2005, San Francisco, CA, 2005, pp. 1056-1063 Vol. 2.

[4] Q. Zhong, "Virtual synchronous machines: a unified interface for grid integration," in IEEE Power Electronics Magazine, vol. 3, no. 4, pp. 18-27, Dec. 2016.

[5] N. Soni, S. Doolla and M. C. Chandorkar, "Improvement of transient response in microgrids using virtual inertia," in IEEE Transactions on Power Delivery, vol. 28, no. 3, pp. 1830-1838, July 2013.

[6] Y. Du, J. M. Guerrero, L. Chang, J. Su and M. Mao, "Modeling, analysis, and design of a frequency-droop-based virtual synchronous generator for microgrid applications," 2013 IEEE ECCE Asia Downunder, Melbourne, VIC, 2013, pp. 643-649.

[7] Z. Song et al., "Small signal modeling and parameter design of virtual synchronous generator to weak grid," 2018 13th IEEE Conference on Industrial Electronics and Applications (ICIEA), Wuhan, 2018, pp. 2618-2624.

[8] T. Shintai, Y. Miura and T. Ise, "Oscillation Damping of a Distributed Generator Using a Virtual Synchronous Generator,"in IEEE Transactions on Power Delivery, vol. 29, no. 2, pp. 668-676, April 2014.

[9] H. Wu et al., "Small-Signal modeling and parameters design for virtual synchronous generators," in IEEE Transactions on Industrial Electronics, vol. 63, no. 7, pp. 4292-4303, July 2016.

[10] L. Zhang, L. Harnefors and H. P. Nee, "Power-Synchronization control of grid-connected voltage-source converters," in IEEE Transactions on Power Systems, vol. 25, no. 2, pp. 809-820, May 2010.

[11] V. Blasko, "Analysis of a hybrid PWM based on modified space-vector and triangle-comparison methods,"in IEEE Transactions on Industry Applications, vol. 33, no. 3, pp. 756-764, May-June 1997.

[12] N. S. Nise, Control Systems Engineering, 6rd ed., John Wiley & Sons, Inc., USA, 2011.